Space-based constraints on the production of nitric oxide by lightning

Randall V. Martin,[1,2] Bastien Sauvage,[1] Ian Folkins,[1] Christopher E. Sioris,[2,3,4] Christopher Boone,[5] Peter Bernath,[5] and Jerry Ziemke[6,7]

Received 25 July 2006; revised 9 November 2006; accepted 13 December 2006; published 11 May 2007.

[1] We interpret observations of trace-gases from three satellite platforms to provide top-down constraints on the production of NO by lightning. The space-based observations are tropospheric NO_2 columns from SCIAMACHY, tropospheric O_3 columns from OMI and MLS, and upper tropospheric HNO_3 from ACE-FTS. A global chemical transport model (GEOS-Chem) is used to identify locations and time periods in which lightning would be expected to dominate the trace gas observations. The satellite observations are sampled at those locations and time periods. All three observations exhibit a maximum in the tropical Atlantic region and a minimum in the tropical Pacific. This wave-1 pattern is driven by injection of lightning NO into the upper troposphere over the tropical continents, followed by photochemical production of NO_2, HNO_3, and O_3 during transport. Lightning produces a broad enhancement over the tropical Atlantic and Africa of $2-6 \times 10^{14}$ molecules NO_2 cm^{-2}, 4×10^{17} molecules O_3 cm^{-2} (15 Dobson Units), and 125 pptv of upper tropospheric HNO_3. The lightning background is 25–50% weaker over the tropical Pacific. A global source of 6 ± 2 Tg N yr^{-1} from lightning in the model best represents the satellite observations of tropospheric NO_2, O_3, and HNO_3.

Citation: Martin, R. V., B. Sauvage, I. Folkins, C. E. Sioris, C. Boone, P. Bernath, and J. Ziemke (2007), Space-based constraints on the production of nitric oxide by lightning, *J. Geophys. Res.*, *112*, D09309, doi:10.1029/2006JD007831.

1. Introduction

[2] Nitrogen oxide radicals ($NO_x \equiv NO + NO_2$) originating from combustion, lightning, and soils largely control tropospheric O_3 production [*Kasibhatla et al.*, 1991; *Penner et al.*, 1991; *Murphy et al.*, 1993; *Jacob et al.*, 1996]. Lightning remains the most uncertain source of NO_x [*Lee et al.*, 1997]. Most estimates of the global lightning NO_x source have employed a bottom-up approach based on estimates of global flash rates and the number of molecules of NO produced per flash [*Price et al.*, 1997a; *Labrador et al.*, 2005]. Top-down constraints based on satellite observations of trace gases could reduce considerably this uncertainty.

[3] Table 1 contains recent estimates of global lightning NO_x production. Global estimates vary by more than an order of magnitude over 1–20 Tg N yr^{-1}. Flash rates explain only a small fraction of this uncertainty. Recent estimates of global flash rates derived from space-based measurements from the Optical Transient Detector (OTD) are 44 ± 5 flashes s^{-1} [*Christian et al.*, 2003], 50–75% of earlier estimates over the last decade. The remaining uncertainty in global estimates from the bottom-up approach arises from the production of NO/flash, for which recent values vary by an order of magnitude, in part reflecting spatial variation in the frequency [*Boccippio et al.*, 2001] and uncertainty in the relative yield [*Ridley et al.*, 2005] of cloud-ground (CG) and intracloud (IC) flashes.

[4] *Levy et al.* [1996] introduced an alternative top-down approach of comparing airborne observations of NO_x and NO_y with a global model simulation and found that this approach yielded a tight constraint on the lightning NO_x source. *Boersma et al.* [2005] extended their method using satellite measurements of tropospheric NO_2 columns from the Global Ozone Monitoring Instrument (GOME). We develop the top-down approach here using global observations of tropospheric NO_2 columns from the Scanning Imaging Absorption Spectrometer for Atmospheric Chartography (SCIAMACHY) satellite instrument [*Bovensmann et al.*, 1999], tropospheric O_3 columns from the Ozone Monitoring Instrument (OMI) [*Levelt et al.*, 2006] and Microwave Limb Sounder (MLS) [*Waters et al.*, 2006] instruments, and upper tropospheric HNO_3 measurements from the Atmospheric Chemistry Experiment Fourier Transform Spectrometer (ACE-FTS) [*Bernath et al.*, 2005]. These multiple species provide three independent constraints on the lightning NO_x source.

[5] A major challenge in interpreting satellite observations of a tropospheric column is ambiguity in the altitude of the gas. Surface sources and free tropospheric sources both

[1]Department of Physics and Atmospheric Science, Dalhousie University, Halifax, Nova Scotia, Canada.
[2]Also at Harvard-Smithsonian Center for Astrophysics, Cambridge, Massachusetts, USA.
[3]Department of Physics and Engineering Physics, University of Saskatchewan, Saskatoon, Saskatchewan, Canada.
[4]Now at Environment Canada, Downsview, Ontario, Canada.
[5]Department of Chemistry, University of Waterloo, Waterloo, Ontario, Canada.
[6]University of Maryland Baltimore County (UMBC), Goddard Earth Sciences and Technology (GEST), Baltimore, Maryland, USA.
[7]Also at NASA Goddard Space Flight Center, Code 613.3, Greenbelt, Maryland, USA.

0148-0227/07/2006JD007831

Table 1. Recent Estimates of Global Lightning NO_x Production

Study	Production Rate, Tg N yr^{-1}	Approach	Flash, s^{-1}	10^{25} atoms, N/flash
Levy et al. [1996]	2–6	Comparison of global model with airborne observations of NO_x and NO_y		
Ridley et al. [1996]	2–5	Extrapolation of airborne measurements of New Mexico storms	100	
Price et al. [1997a]	12 (5–20)[a]	Lightning physics	70–100	25 (4–105)[b]
Price et al. [1997b]	13 (5–25)	Constraints from atmospheric electricity		
Huntrieser et al. [1998]	4 (0.3–22)	Extrapolation of airborne measurements of storms in Europe		4–30
H. Wang et al. [1998]	3–8	Bottom-up from laboratory measurements	30–100	3
Y. Wang et al. [1998]	3	Comparison of global model with airborne observations in North Atlantic		
Nesbitt et al. [2000]	0.9	Global satellite flash counts	57	2 (1–6)
Bond et al. [2002]	6 (0.5–9)	LIS flash counts	45	20 (7–70)
Huntrieser et al. [2002]	3 (1–20)	Extrapolation of airborne measurements of storms in Europe	65	8
Martin et al. [2002b]	6	Comparison of global model with O_3 from TOMS and sondes		
Beirle et al. [2004]	3 (0.8–14)	Extrapolation of GOME NO_2 and LIS observations over Australia	63	6 (2–30)
Ridley et al. [2004]	1–8	Extrapolation of measurements of Florida thunderstorms	44	3–23
Boersma et al. [2005]	1–6	Analysis of GOME NO_2 observations in southern tropics		
Labrador et al. [2005]	<20	Comparison of global model with airborne observations of NO_x		
Beirle et al. [2006]	2 (0.6–5)	Extrapolation of GOME measurements of NO_2 in the Gulf of Mexico	44	5 (2–14)
This work	6 (4–8)	Comparison of global model with satellite observations of NO_2, O_3, and HNO_3		

[a]The reported estimate range is given in parentheses.
[b]Represents the weighted average for intercloud and cloud-ground flashes.

contribute to column enhancements. Figure 1 shows a current estimate of the distribution of NO_x production by lightning and other sources. Most regions with a substantial lightning NO_x source also contain considerable emissions from other sources, confounding a simple correlation between the column observation and lightning flashes. However, one major difference between the production of NO_x from lightning and other sources is their altitude. Simulations with cloud resolving models suggest that most lightning NO_x is deposited above 7 km [*Pickering et al.*, 1998; *Skamarock et al.*, 2003] where the lifetimes of NO_x, HNO_3, and O_3 are 5–10 times longer than in the lower troposphere. In the tropics, convection of NO_x from surface sources is expected to make a minor contribution to upper tropospheric NO_x compared with lightning NO_x emissions [*Levy et al.*, 1999]. Lightning NO_x would be expected to influence a much broader region than surface sources [*Lamarque et al.*, 1996]. An upper tropospheric airmass will be advected along a different trajectory than a lower tropospheric airmass that is influenced by surface emissions. *Boersma et al.* [2005] introduced the idea of a masking scheme to extract the lightning signal by minimizing the interference of surface NO_x sources on satellite observations.

[6] In this work we use a global chemical transport model (GEOS-Chem) to identify the locations, regions, and species that are dominated by the effects of lightning NO_x. Section 2 introduces the GEOS-Chem model. Section 3 compares the satellite observations of tropospheric NO_2, O_3, and HNO_3 with the model simulation in those regions. Conclusions are in section 4.

2. GEOS-Chem Model

[7] We use the GEOS-Chem global three-dimensional (3-D) chemical transport model to account for the photochemical evolution and transport of NO_x. The simulation is driven by assimilated meteorological data from the Goddard Earth Observing System (GEOS-4) at the NASA Global

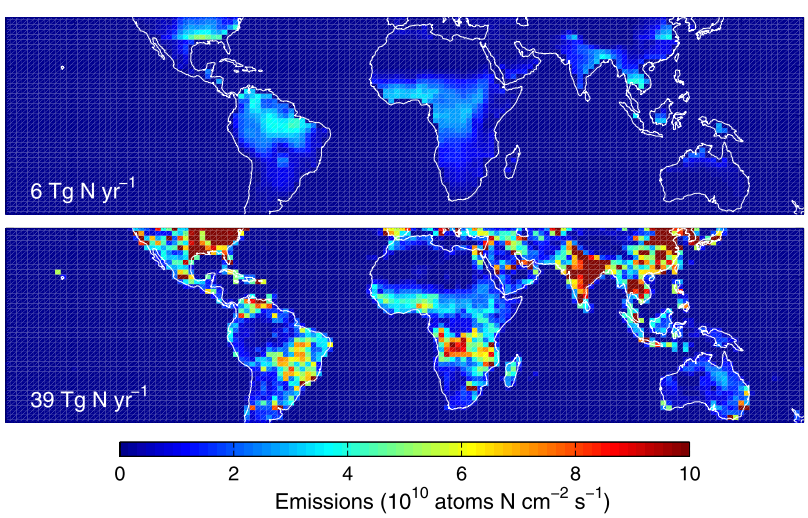

Figure 1. Annual mean NO_x emissions used in the standard GEOS-Chem simulation from (top) lightning and (bottom) all other sources including fossil fuel combustion, biomass burning, biofuels, and soils.

Modeling and Assimilation Office (GMAO). We use here version 7-03-03 of GEOS-Chem (www-as.harvard.edu/chemistry/trop/geos) with additional midlatitude lightning NO_x as described below. The GEOS-Chem model includes a detailed simulation of tropospheric ozone-NO_x-hydrocarbon chemistry as well as of aerosols and their precursors. The ozone-NO_x-hydrocarbon simulation was first described by *Bey et al.* [2001] with updates by *Fiore et al.* [2002] and *Martin et al.* [2002b, 2003b]. The model presently includes sulfate, nitrate, ammonium, black carbon, organic carbon, mineral dust, and sea salt [*Park et al.*, 2003; *Park et al.*, 2004; *Alexander et al.*, 2005; *Fairlie et al.*, 2006]. The aerosol and gaseous simulations are coupled through formation of sulfate and nitrate, $HNO_3(g)/NO_3^-$ partitioning of total inorganic nitrate, heterogeneous chemistry on aerosols [*Jacob*, 2000; *Evans and Jacob*, 2005], and aerosol effects on photolysis rates [*Martin et al.*, 2003b].

[8] Figure 1 shows the annual global distribution of NO_x emissions in GEOS-Chem for all sources. Anthropogenic NO_x emissions are based on the Global Emission Inventory Activity (GEIA) [*Benkovitz et al.*, 1996] as described by *Bey et al.* [2001]. Soil NO_x emissions are computed using a modified version of the algorithm of *Yienger and Levy* [1995] with the canopy reduction factors described by *Y. Wang et al.* [1998]. The biomass burning inventory is seasonally varying and is based on satellite observations of fires over 1996–2000 from the Along Track Scanning Radiometer (ATSR) as derived by *Duncan et al.* [2003]. Emissions of lightning NO_x are linked to deep convection following the parameterization of *Price and Rind* [1992] with vertical profiles from *Pickering et al.* [1998] as implemented by *Y. Wang et al.* [1998]. The midlatitude lightning NO_x source is increased here by a factor of four to 1.6 Tg N yr^{-1} following *Hudman et al.* [2007] and *Martin et al.* [2006] to correct a model bias in simulated NO_x versus INTEX-A aircraft observations, to be consistent with NO production per flash estimates from recent cloud-scale modeling [*DeCaria et al.*, 2005; *Pickering et al.*, 2006], and to account for recent observational evidence that midlatitude lightning may produce more NO per flash than tropical lightning [*Huntrieser et al.*, 2006]. The model chemical fields have been evaluated versus in situ and satellite observations throughout the tropics [*Bey et al.*, 2001; *Chandra et al.*, 2002; *Martin et al.*, 2002b; *Chandra et al.*, 2003; *Martin et al.*, 2003a; *Jaeglé et al.*, 2005; *Kim et al.*, 2005; *Folkins et al.*, 2006; *Liu et al.*, 2006; *Sauvage et al.*, 2007a].

[9] We conduct eight sensitivity simulations with variable lightning source strength, or with NO_x emissions excluded from either biomass burning or soils to examine the effect of these sources. Sensitivity simulations are conducted over May 2004 to April 2005, following a 4-month spinup. Two additional sensitivity studies are used to assess the robustness of the conclusions to spatial variation in the lightning source. Estimates of the relative vertical distribution of lightning NO_x is affected by uncertainty in the NO_x production per flash for intracloud (P_{IC}) and cloud-ground (P_{CG}) flashes. The vertical profiles from *Pickering et al.* [1998] used in the standard simulation were determined for a P_{IC}/P_{CG} ratio of 0.1, based on the work of *Price et al.* [1997a]. There is evidence for a P_{IC}/P_{CG} ratio of 0.5–1 [*Gallardo and Cooray*, 1996; *DeCaria et al.*, 2000; *Zhang et al.*, 2003; *Fehr et al.*, 2004; *DeCaria et al.*, 2005; *Ott et al.*, 2007]. One sensitivity study uses a P_{IC}/P_{CG} ratio of 0.75 in which the additional NO_x from intracloud flashes is distributed within the cloud anvil.

[10] *Allen and Pickering* [2002] found that the *Price and Rind* [1992] lightning parameterization does not fully capture the observed distribution of lightning activity. We conduct another sensitivity study in which the spatial distribution of lightning NO_x production is rescaled to match 10 years of seasonally varying observations of lightning flashes from the OTD and the Lightning Imaging Sensor (LIS) as implemented by *Sauvage et al.* [2007a].

3. Top-Down Constraints on Lightning NO_x Emissions

[11] Satellite retrievals of tropospheric NO_2 columns, tropospheric O_3 columns, and upper tropospheric HNO_3 provide three independent constraints on the production of NO from lightning. We examine each species in turn.

3.1. Analysis of Tropospheric NO_2 Columns

[12] The SCIAMACHY instrument on board the ENVISAT satellite provides the capability for global retrieval of atmospheric NO_2 columns through observation of global backscatter [*Bovensmann et al.*, 1999]. The satellite was launched in March 2002 into a Sun-synchronous orbit, crossing the equator at about 1000 LT in the descending node. The SCIAMACHY instrument observes the atmosphere in the nadir view with a typical surface spatial resolution of 30 km along track by 60 km across track. Global coverage is achieved every 6 days.

[13] We use cloud-filtered (cloud radiance fraction <0.5) tropospheric NO_2 columns retrieved by *Martin et al.* [2006] for May 2003 to April 2005. The retrieval involves a spectral fit over 429–452 nm to produce total slant columns, removal of stratospheric NO_2 columns using SCIAMACHY observations over the Pacific, and an air mass factor calculation to correct for atmospheric scattering. The data have been validated with in situ airborne observations of NO_2 over and downwind of North America as part of the ICARTT campaign. The retrieval uncertainty is $\pm(5 \times 10^{14}$ molecules cm^{-2} + 30%) for cloud-filtered scenes with larger uncertainty for cloudy scenes. The omission of cloudy scenes is of little consequence for our analysis due to the long upper tropospheric NO_x lifetime of 5–10 days as inferred by *Jaeglé et al.* [1998].

[14] Figure 2 shows a seasonal average of cloud-filtered SCIAMACHY tropospheric NO_2 columns. Tropospheric NO_2 columns are strongly correlated with surface emissions [*Martin et al.*, 2003a; *Toenges-Schuller et al.*, 2006]. NO_2 columns are largest in winter over industrial regions due to seasonal variation in the NO_x lifetime [*Velders et al.*, 2001]. The seasonal variation of tropical NO_2 columns reflects biomass burning and soil NO_x emissions [*Jaeglé et al.*, 2005]. Identification of a lightning signal in satellite observations of NO_2 columns is complicated by the higher measurement sensitivity to NO_x in the lower troposphere than in the upper troposphere [*Martin et al.*, 2002a], resulting from the factor of 25 increase in the NO/NO_2 ratio from the surface to the tropopause [*Bradshaw et al.*, 1999] that is driven by the temperature dependence of the $NO + O_3$ reaction.

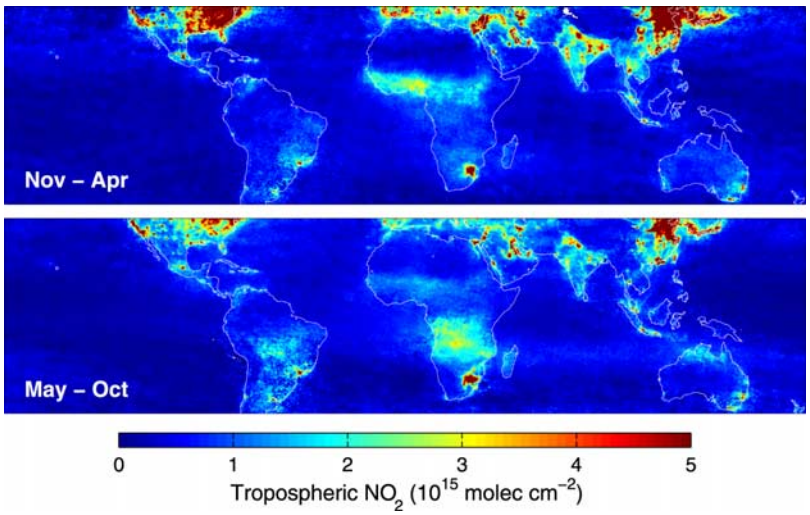

Figure 2. Mean tropospheric NO_2 columns retrieved from the SCIAMACHY satellite instrument for (top) November–April and (bottom) May–October. Scenes where clouds or snow dominate solar backscatter have been excluded from the average to reduce retrieval uncertainty. Data from *Martin et al.* [2006].

[15] The interpretation of satellite observations of tropospheric columns warrants clarification of the tropical tropopause. The level of zero radiative heating occurs at 14–15 km, above which air either mixes with the extratropical stratosphere or slowly ascends through the thermal tropopause at 16–17 km and into the tropical stratosphere [*Highwood and Hoskins*, 1998; *Folkins et al.*, 1999]. We refer to the tropopause as the thermal tropopause and to tropospheric columns as values below the thermal tropopause.

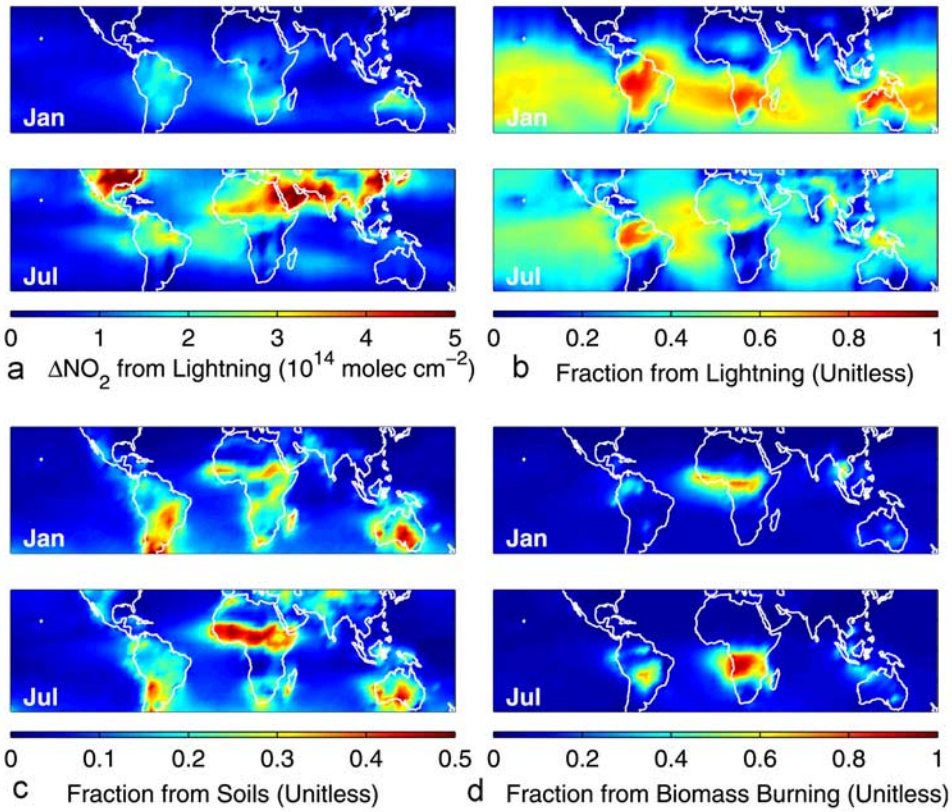

Figure 3. Sensitivity of simulated tropospheric NO_2 columns to NO_x emissions from lightning, soils, and biomass burning for January and July. (a) Shown is the NO_2 column due to lightning NO_x emissions as determined by the difference between the standard simulation and a simulation that excludes lightning NO_x emissions. Also shown is the fraction of the simulated tropospheric NO_2 column from (b) lightning, (c) soils, and (d) biomass burning.

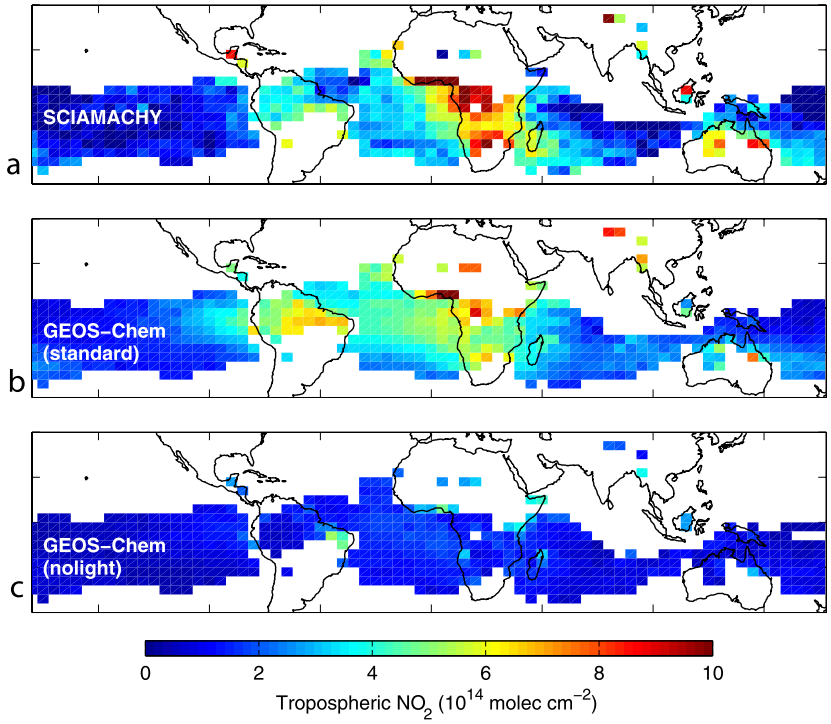

Figure 4. Annual average of tropospheric NO_2 columns at locations and times in which more than 60% of the simulated NO_2 column is from lightning, and less than 25% of the simulated NO_2 column is from any surface NO_x source (soils, biomass burning, fossil fuels, or biofuel). White areas indicate regions where these thresholds were not met. Shown are (a) data retrieved from the SCIAMACHY satellite instrument, (b) the standard simulation with 6 Tg N yr^{-1} from lightning, and (c) a simulation without lightning NO_x emissions.

[16] Given the strong relationship of tropospheric NO_2 columns with surface emissions, we use the GEOS-Chem model for guidance in identifying locations where a lightning influence would be expected. Figure 3 shows the sensitivity of tropospheric NO_2 columns to NO_x emissions from either lightning, soils, or biomass burning as determined from the difference between the standard simulation and sensitivity simulations that exclude either source. Figure 3a shows that the largest lightning-induced enhancements of the tropospheric NO_2 column are found over and downwind of active convective regions. The maximum monthly mean enhancements are comparable to the SCIAMACHY retrieval uncertainty.

[17] Figure 3b shows the fraction of the NO_2 column from lightning. This fraction is anticorrelated ($r = -0.49$) with the simulated tropical tropospheric NO_2 column, reflecting the greater sensitivity of SCIAMACHY to NO_x in the lower troposphere than in the upper troposphere. The largest relative contributions from lightning are found over convective regions with negligible surface sources. Lightning has the broadest relative influence during January–April when flashes are most frequent in the Southern Hemisphere and when biomass burning is largely confined to the Northern Hemisphere. Lightning makes the weakest relative contribution during July–October when lightning is active in the Northern Hemisphere where there are numerous anthropogenic sources.

[18] Figures 3c and 3d show the fraction of the tropospheric NO_2 column from soil and biomass burning emissions. The largest fractions from soils are found over tropical savannas during the wet season. *Jaeglé et al.* [2004] attributed GOME observations of tropospheric NO_2 column enhancements over northern Africa to rain-induced emissions of NO from soils. A large contribution from biomass burning of more than 50% is found over northern equatorial Africa during January and over central Africa during July. Soil and biomass burning emissions make a small contribution (typically <25%) to tropospheric NO_2 columns over oceans. The sum of the fractional contributions from these sources can exceed 100% due to nonlinearities.

[19] We sample the SCIAMACHY data at locations and months in which GEOS-Chem simulations indicate that more than 60% of the NO_2 column is from lightning, and less than 25% of the NO_2 column originates from any surface NO_x source (soils, biomass burning, fossil fuel, or biofuel). These thresholds retain 15% of the tropical SCIAMACHY data. Most land regions are excluded by these thresholds, since surface NO_x sources often dominate the NO_2 column over land.

[20] Figure 4a shows the annual average of the filtered SCIAMACHY tropospheric NO_2 columns. The largest enhancements are found over central Africa reflecting intense lightning activity [*Christian et al.*, 2003]. A broad enhancement of $3-6 \times 10^{14}$ molecules cm^{-2} is evident over the tropical Atlantic and Indian Oceans, reflecting upper tropospheric transport from continental regions. Lightning is the dominant source of reactive nitrogen transported into the tropical Atlantic in a numerical simulation by *Moxim*

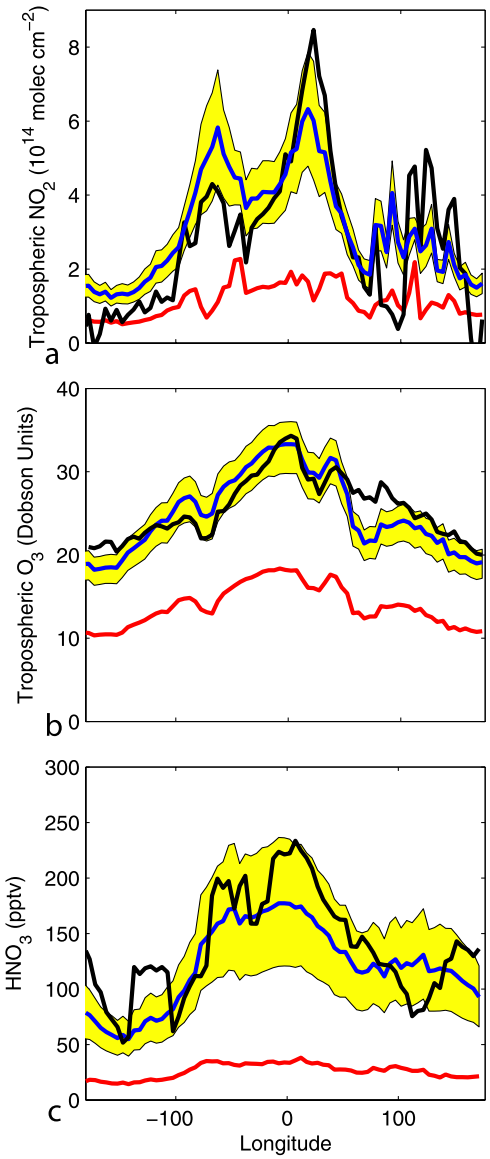

Figure 5. Meridional average of annual mean trace gas concentrations for locations and months that are dominated by the effects lightning NO_x. Shown are (a) tropospheric NO_2 columns for locations and months in which more than 60% of the tropospheric NO_2 column is from lightning, and less than 25% of the NO_2 column from any surface NO_x source, (b) the tropospheric O_3 column averaged over locations and months in which more than 40% of the simulated concentrations are from lightning NO_x, and (c) the HNO_3 mixing ratio between 200 and 350 hPa averaged over locations and months in which more than 60% of the simulated concentrations are from lightning NO_x. Black lines indicate satellite observations. Blue lines indicate the standard simulation with 6 Tg N yr^{-1} from lightning. The boundaries of the yellow shaded regions indicate sensitivity simulations of 4 and 8 Tg N yr^{-1} from lightning. Red lines indicate the simulation without lightning NO_x emissions.

and Levy [2000]. Previous analyses of tropospheric NO_2 columns retrieved from GOME also found evidence of lightning NO_x over the tropical Atlantic [*Richter and Burrows*, 2002; *Edwards et al.*, 2003; *Boersma et al.*, 2005].

[21] Figure 4b shows the annual average of simulated tropospheric NO_2 columns, sampled at the same time and location as the SCIAMACHY measurements. The modeled NO_2 columns are broadly consistent with the SCIAMACHY data (r = 0.75, n = 1937, bias = 8%). The simulation also exhibits a broad maximum over the tropical Atlantic Ocean and a broad minimum over the tropical Pacific Ocean. The simulation overestimates the lightning signal over South America and underestimates the lightning signal over Africa, common problems for models using the *Price and Rind* [1992] parameterization [*Allen and Pickering*, 2002]. This bias is reduced in the sensitivity simulation in which lightning flashes are rescaled to the OTD/LIS observations.

[22] Figure 4c shows the annual average of tropospheric NO_2 columns in the simulation without lightning NO_x emissions. Tropospheric NO_2 columns in this simulation are biased low by 60% with respect to the SCIAMACHY data. Comparison with Figure 4b reveals that lightning largely explains the broad wave-1 pattern in the SCIAMACHY NO_2 columns.

[23] Figure 5a compares the meridional average of all the tropospheric NO_2 columns in Figure 4. Both the SCIAMACHY NO_2 columns and the standard simulation show enhancements in the tropical Atlantic, relative to the tropical Pacific. No such pattern is found in the simulation without lightning NO_x emissions. Emissions of 4–8 Tg N yr^{-1} would best represent the SCIAMACHY data over most of the tropics. The magnitude of the annual mean lightning signal in the tropospheric NO_2 observations is about 2–6 $\times$ 10^{14} molecules cm^{-2}, comparable to the local uncertainty of about 5 $\times$ 10^{14} molecules cm^{-2} in the SCIAMACHY tropospheric NO_2 retrievals. However, it is likely that the retrieval error is reduced for the spatial and temporal mean examined here.

3.2. Analysis of Tropospheric Ozone Columns

[24] The OMI and MLS instruments were launched in July 2004 on board the Aura spacecraft into a polar Sun-synchronous orbit [*Schoeberl et al.*, 2004]. OMI is a nadir-scanning instrument that detects backscattered solar radiance over 270–500 nm to measure column O_3 with near global coverage at a resolution of 13 km $\times$ 24 km at nadir [*Levelt et al.*, 2006]. The EOS MLS instrument is a thermal-emission microwave limb sounder that measures vertical profiles of mesospheric, stratospheric, and upper tropospheric O_3 from limb scans ahead of the Aura satellite [*Froidevaux et al.*, 2006; *Waters et al.*, 2006]. *Ziemke et al.* [2006] combined measurements from both instruments to retrieve daily tropospheric O_3 columns with a measurement uncertainty of 5 Dobson Units (DU) as determined by comparison with ozonesondes.

[25] Figure 6 shows tropospheric O_3 columns retrieved from the OMI and MLS instruments for January and July. A persistent wave-1 pattern is found in the southern tropics, with a maximum in the tropical Atlantic and a minimum in the tropical Pacific throughout the year [*Fishman et al.*, 1990; *Shiotani*, 1992; *Ziemke et al.*, 1996; *Hudson and Thompson*, 1998; *Thompson et al.*, 2003; *Sauvage et al.*, 2006]. The minimum in the tropical Pacific reflects the rapid destruction of O_3 in the marine boundary layer [*Piotrowicz et al.*, 1991; *Kley et al.*, 1996] coupled with

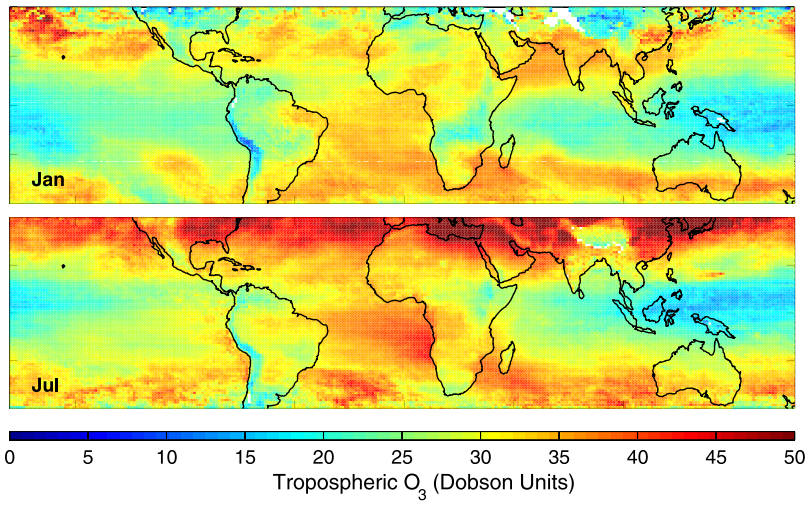

Figure 6. Tropospheric ozone columns retrieved from the Ozone Monitoring Instrument (OMI) and Microwave Limb Sounder (MLS) for (top) January 2005 and (bottom) July 2005. Data from *Ziemke et al.* [2006].

the negative tendency of deep convection on the O_3 column [*Lelieveld and Crutzen*, 1994]. The persistent maximum over the tropical Atlantic reflects the integrated effect on O_3 of lightning emissions over the tropical continents [*Jacob et al.*, 1996; *Martin et al.*, 2002b; *Sauvage et al.*, 2007b], coupled with seasonal enhancements from biomass burning [*Thompson et al.*, 1996; *Jenkins et al.*, 1997]. The enhancement in the northern hemisphere during July is driven by photochemical production from anthropogenic emissions [*Fishman and Brackett*, 1997]. Enhancements at ±30° are due to a combination of subsidence from the stratosphere and photochemical production [*Li et al.*, 2002; *Jing et al.*, 2005].

[26] Figure 7 shows the simulated sensitivity of tropospheric O_3 columns to lightning NO_x emissions. Lightning makes a broad contribution to tropospheric O_3 columns throughout the tropics reflecting the upper tropospheric O_3 lifetime of several weeks. A particularly large O_3 column enhancement from lightning is apparent during January in the southern tropical Atlantic, contributing to the north-south oceanic gradient that was highlighted by *Thompson et al.* [2000]. Weaker enhancements from lightning are found over the Middle East during July [*Li et al.*, 2001] and in the subsiding branches of the Hadley Circulation near ±30°. Lightning makes a smaller relative contribution to the tropospheric O_3 column during July when biomass burning emissions are more abundant in the southern hemisphere and when lightning is predominantly in the northern hemisphere where anthropogenic sources dominate.

[27] Figure 8a shows the annual average over September 2004 to August 2005 of the OMI/MLS tropospheric O_3 columns at locations and times in which more than 40% of the simulated column is from lightning. This threshold retains 15% of the tropical OMI/MLS observations. Only 0.1% of the remaining observations would be affected by an additional threshold of 25% on the O_3 column fraction from surface sources. Figure 8b shows the annual average of the standard simulation sampled at the same locations and months as the OMI/MLS data. There is a high degree of consistency between the simulated and satellite data (r = 0.85, n = 1953, bias = −1%). Figure 8c shows tropospheric

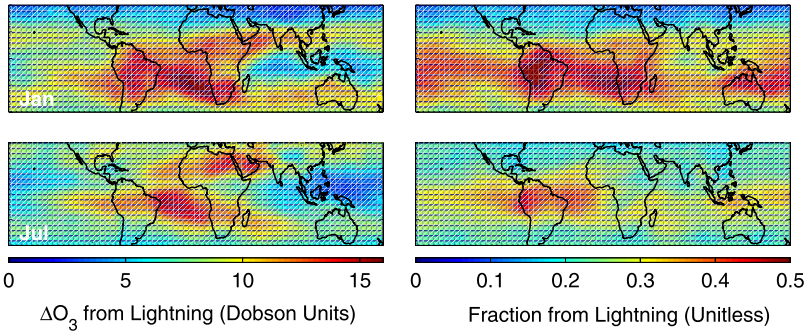

Figure 7. Sensitivity of tropospheric ozone columns to lightning NO_x emissions for (top) January and (bottom) July. The left column indicates the tropospheric ozone column due to lightning NO_x emissions as determined by the difference between the standard simulation and a simulation that excludes lightning NO_x emissions. The right column indicates the corresponding fraction of the tropospheric ozone column from lightning NO_x emissions.

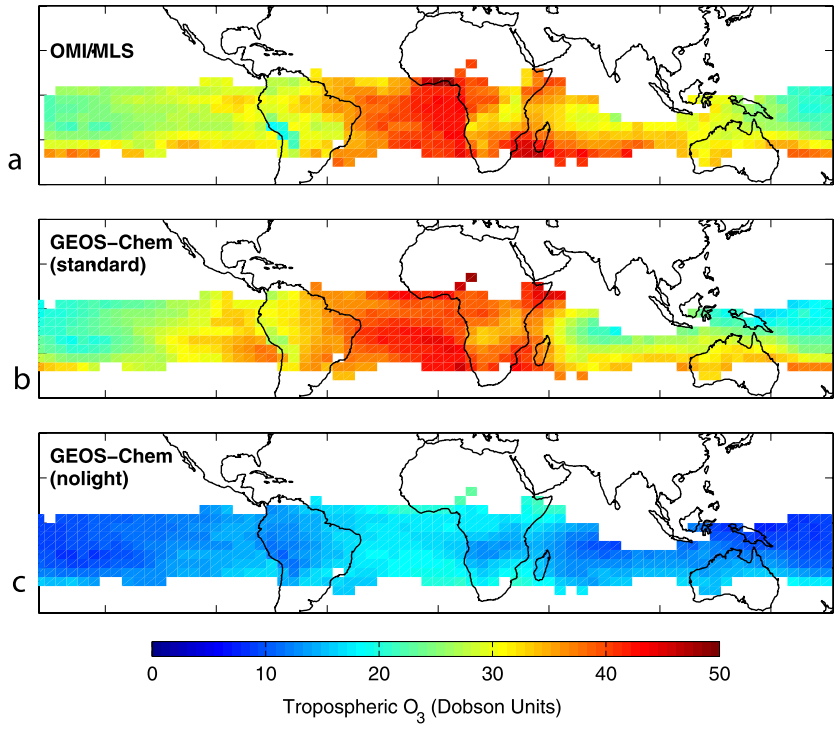

Figure 8. Annual average of tropospheric ozone columns at locations and times in which GEOS-Chem simulations yield more than 40% of the tropospheric ozone column from lightning. White areas indicate regions where these thresholds were not met. Shown are (a) data determined from the OMI and MLS satellite instruments, (b) the standard simulation with 6 Tg N yr^{-1} from lightning, and (c) a simulation without lightning NO_x emissions.

O_3 columns for the simulation without lightning NO_x emissions, revealing a large negative bias of 45% versus the OMI/MLS observations. The magnitude of the lightning signal of 10–15 DU, as determined by the difference between the standard simulation and the simulation without lightning, is 2–3 times greater than the retrieval uncertainty.

[28] Figure 5b shows the meridional average of the tropospheric O_3 columns in Figure 8. Lightning NO_x production of 4–6 Tg N yr^{-1} would best represent the OMI/MLS observations in the Atlantic, while a rate of 6–8 Tg N yr^{-1} would best represent observations in the Pacific.

3.3. Analysis of Upper Tropospheric HNO_3

[29] The ACE-FTS instrument [*Bernath et al.*, 2005] was launched on board the SCISAT-1 spacecraft into a low Earth orbit (altitude 650 km, inclination 74°) in August 2003.

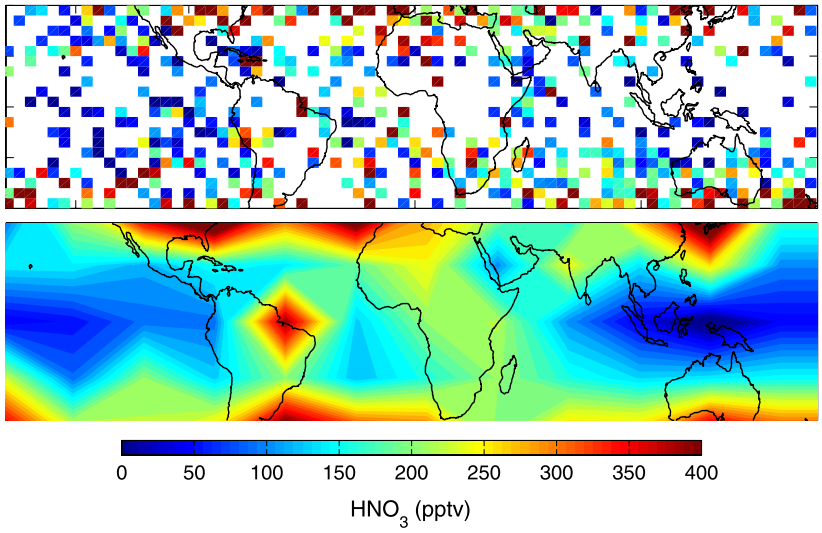

Figure 9. Mean HNO_3 retrieved from the ACE-FTS satellite instrument over 200–350 hPa for March 2004 to February 2006 inclusive. The data are binned onto a 4° latitude by 5° longitude grid in the top panel and onto a 20° latitude by 30° longitude grid in the bottom panel. Data from *Boone et al.* [2005].

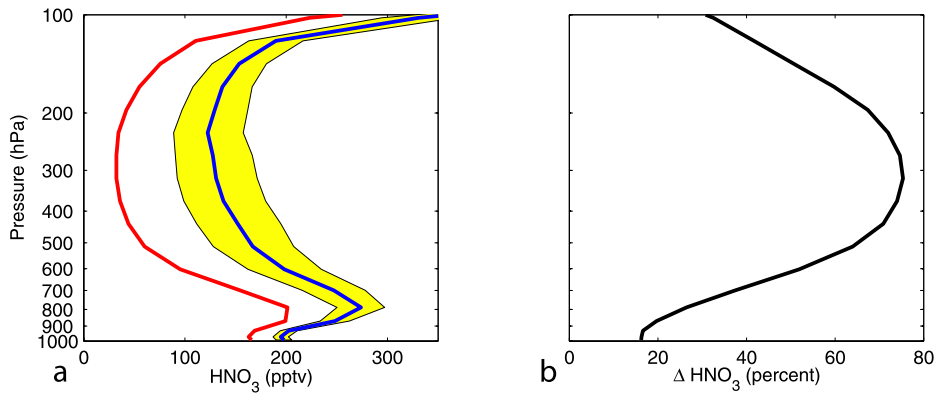

Figure 10. Vertically resolved sensitivity of the tropical (30°S–30°N) HNO_3 concentration to NO_x emissions from lightning, showing (a) the annual mean tropical HNO_3 mixing ratio. The blue line indicates the standard simulation. The boundaries of the yellow shaded region indicate sensitivity simulations of 4 and 8 Tg N yr^{-1} from lightning. The red line indicates simulated values in the simulation without lightning NO_x emissions. Also shown is (b) the fraction of HNO_3 from lightning as determined by the difference between the standard simulation and a simulation without lightning NO_x emissions.

The ACE-FTS instrument is a high spectral resolution (0.02 cm^{-1}) Fourier Transform Spectrometer operating over 750–4400 cm^{-1} (2.2–13.3 μm). From the ACE-FTS solar occultation measurements, HNO_3 profiles are retrieved with an altitude resolution of 3–4 km [*Boone et al.*, 2005]. The retrievals employ HNO_3 spectral features in the ranges 860–910 cm^{-1} and 1690–1730 cm^{-1}. The typical measurement uncertainty in the upper troposphere is 35 pptv. The data used here are research retrievals for HNO_3, a refinement of the version 2.2 ACE-FTS data set.

[30] Figure 9 shows the average of HNO_3 concentrations over 200–350 hPa from ACE-FTS for March 2004 to February 2006 inclusive. Enhancements are found poleward of 25° due to a combination of seasonally varying tropospheric and stratospheric sources. Consistently low values are seen over the Pacific Ocean. As with NO_2 and O_3, we use the GEOS-Chem model to provide insight into the processes affecting the HNO_3 distribution.

[31] We first examine the vertical sensitivity of HNO_3 to lightning NO_x emissions. Figure 10a shows HNO_3 concentrations for simulations with and without lightning. A broad minimum in the tropical upper troposphere has been attributed to convective outflow of air depleted of this highly soluble species [*Folkins et al.*, 2006]. The increase in HNO_3 with decreasing pressure represents an increasing stratospheric contribution, while the increase toward the surface is driven by photochemical production of HNO_3 during subsidence. The role of surface NO_x sources increases markedly below 600 hPa. Figure 10b shows that oxidation of lightning NO_x explains nearly 80% of HNO_3 concentrations over 200–350 hPa. We focus our attention on this region.

[32] Figure 11 shows the calculated horizontal sensitivity of HNO_3 concentrations to lightning NO_x. The left column of Figure 11 indicates pronounced enhancements over and downwind of convective regions, especially in the southern tropics during January. The right column of Figure 11 indicates that during January lightning NO_x explains 80% of HNO_3 mixing ratios over a broad region south of 25°N, with stratospheric NO_y making a larger contribution further north. During July, stratospheric NO_y plays a more important role at these pressures south of 25°S. Airborne measurements in the upper troposphere provide evidence that HNO_3 increases the relative humidity in low-temperature cirrus clouds [*Gao et al.*, 2004]. The pronounced contribution of lightning to upper tropospheric HNO_3 found here suggests that a hypothesized increase in lightning NO_x

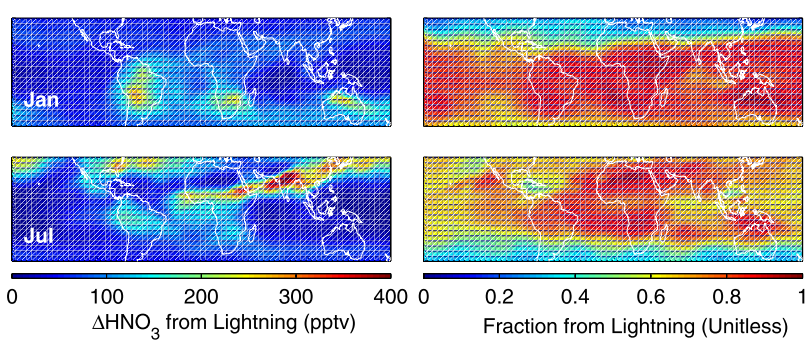

Figure 11. Sensitivity of HNO_3 concentrations over 200–350 hPa to lightning NO_x emissions for (top) January and (bottom) July. The left column shows the HNO_3 mixing ratio due to lightning NO_x, as determined by the difference between the standard simulation and a simulation without lightning NO_x emissions. The right column shows the corresponding fraction of the HNO_3 mixing ratio from lightning.

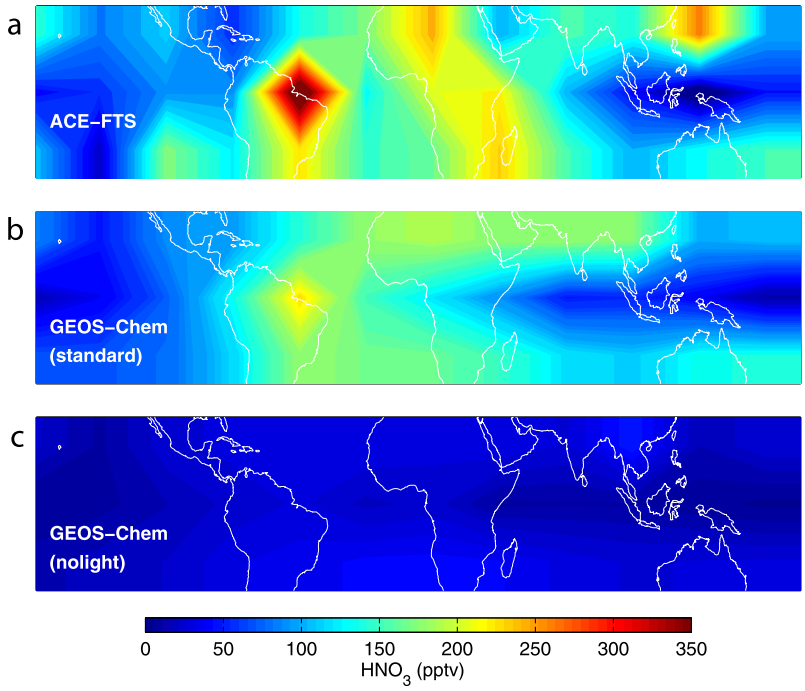

Figure 12. Annual average of the HNO_3 mixing ratio at locations and times in which more than 60% of the simulated HNO_3 concentration is from lightning. Shown are (a) data retrieved from the ACE satellite instrument, (b) the standard simulation with 6 Tg N yr^{-1} from lightning, and (c) a simulation without lightning NO_x emissions.

emissions from climate change [*Price and Rind*, 1994] could have implications for upper tropospheric water vapor.

[33] Figure 12 shows the HNO_3 mixing ratio at locations and times in which more than 60% of the simulated HNO_3 is from lightning. This threshold retains 83% of the tropical ACE-FTS measurements while eliminating the seasonally varying stratospheric air poleward of 25°. The measured and simulated HNO_3 mixing ratios in Figures 12a and 12b are generally consistent (r = 0.75, n = 360, bias = −12%). The simulation underestimates observed upper tropospheric HNO_3 over South America and Africa. However, both the simulation and the observations exhibit a maximum in the tropical Atlantic and a minimum in the tropical Pacific. This wave-1 pattern reflects the frequent injection of HNO_3 depleted air into the upper troposphere of the tropical Pacific, coupled with photochemical production during transport to the tropical Atlantic as part of the Walker circulation. Figure 12c shows that HNO_3 mixing ratios in the simulation without lightning NO_x emissions are only 1/5th of the observations.

[34] Figure 5c shows the meridional average of the upper tropospheric HNO_3 in Figure 12. The simulation with 6 Tg N yr^{-1} from lightning best represents the ACE-FTS observations over most of the world. The strength of the lightning signal in the observations ranges from a minimum of 50 pptv over the western Pacific Ocean to 200 pptv over the tropical Atlantic, exceeding the typical ACE-FTS measurement precision of 35 pptv.

4. Discussion

[35] On balance, all three measurements yield a top-down estimate on the lightning NO_x source of 4–8 Tg N yr^{-1}, with 6 Tg N yr^{-1} being most likely. Potential errors in the simulations used to reach this conclusion are reduced by using three different trace gases with lifetimes ranging from several days for NO_x to several weeks for O_3 and HNO_3. Varying the thresholds used to filter the observations has little effect on the estimate. The sensitivity simulation in which the spatial distribution of lightning flashes is scaled to observations from the OTD and LIS instruments has negligible implications for the top-down estimate for all three trace gases, also supporting the conclusion. Annual mean tropospheric O_3 columns over the regions affected by lightning in the sensitivity simulation with enhanced intracloud lightning exhibit little difference (<1 DU) with the standard simulation, again supporting the conclusion. The small O_3 column enhancement in the simulation with enhanced intracloud lightning reflects compensating changes in upper and lower tropospheric O_3 and in its regional distribution. *Sauvage et al.* [2007a] further discuss the implications of both sensitivity simulations on tropospheric O_3. The weak interannual variation in tropical tropospheric O_3 columns of less than 10% found by *Ziemke and Chandra* [1999] implies a similarly small interannual variation in the lightning NO_x source.

[36] The global estimate of 6 ± 2 Tg N yr^{-1} derived here is well within the range of recent estimates in Table 1. Our estimate is also consistent with the value of 5 ± 3 Tg N yr^{-1} that is used in numerous chemical transport models as summarized by *Zhang et al.* [2003]. A global source strength of less than 4 Tg N yr^{-1} or greater than 8 Tg N yr^{-1} would imply gross errors in current simulations of tropospheric O_3 and reactive nitrogen.

[37] The sensitivity simulation with enhanced intracloud lightning NO_x indicates that tropospheric NO_2 columns and

upper tropospheric HNO_3 concentrations could provide insight into the vertical profile of NO_x emissions. Owing to the increasing NO/NO_2 ratio with altitude, tropospheric NO_2 columns in the simulation with enhanced intracloud lightning are about half of those in the standard simulation, well below the local retrieval uncertainty. In contrast, upper tropospheric HNO_3 concentrations in the simulation with enhanced intracloud lightning are 50–100% larger than in the standard simulation. These divergent effects could imply that in the tropics cloud-ground lightning releases more NO_x than intracloud lightning. *Sauvage et al.* [2007a] similarly find that enhanced intracloud lightning NO_x reduces the consistency of simulated O_3 versus measured vertical profiles from aircraft and ozonesondes. However, if enhanced tropical intracloud lightning is appropriate, two possible explanations for the bias in simulated HNO_3 are an underestimate in the GEOS-4 cloud mass flux detrainment profile [*Folkins et al.*, 2006], or the uptake of HNO_3 by ice in the upper troposphere [e.g., *Abbatt*, 1997; *Zondlo et al.*, 1997]. These coupled issues should be revisited with improved representations of vertical transport, when the existing uncertainty [*Ullerstam et al.*, 2005; *von Kuhlmann and Lawrence*, 2006] in the ice uptake process is reduced, and when the next generation of vertical profiles of lightning NO_x production become available.

[38] The top-down estimate inferred here is based largely on tropical measurements. Included in this global estimate is a northern midlatitude lightning NO_x source of 1.6 Tg N yr^{-1} that is based on recent evidence from aircraft, ozonesonde, and satellite observations as part of the ICARTT and STERAO-A campaigns [*DeCaria et al.*, 2005; *Cooper et al.*, 2006; *Hudman et al.*, 2007; *Martin et al.*, 2006; *Pickering et al.*, 2006]. Recent estimates of the number of moles of NO released per flash over Germany are 70–80% of the North American values [*Fehr et al.*, 2004; *Ott et al.*, 2007] that were used for the midlatitude estimate. Future refinement of the midlatitude lightning NO_x source will propagate into the global estimate.

[39] The OMI instrument also provides the capability for retrieval of tropospheric NO_2 columns [e.g. *Bucsela et al.*, 2006]. Unfortunately, the OMI tropospheric NO_2 product was not available to us at the time of this analysis. Future extension of this approach to use tropospheric NO_2 columns from OMI could benefit from its small footprint in the nadir and daily global coverage.

5. Conclusions

[40] We have analyzed space-based observations of tropospheric NO_2 columns from SCIAMACHY over 2003–2005, tropospheric O_3 columns from OMI and MLS over 2004–2005, and upper tropospheric HNO_3 from ACE-FTS over 2004–2006 to provide top-down constraints on lightning NO_x emissions. A global chemical transport model (GEOS-Chem) was used to identify the locations and months in which lightning would be expected to make a significant contribution to each species. The satellite retrievals were sampled at those locations and months for comparison with model simulations using lightning NO_x emissions of different magnitudes. This approach exploits the role of transport and photochemistry in separating the effect of lightning NO_x from surface NO_x sources. Particular attention was devoted to excluding regions of biomass burning and soil NO_x emissions that could be misinterpreted as a lightning signal in the SCIAMACHY NO_2 columns.

[41] All three filtered satellite datasets revealed a prominent wave-1 pattern with a maximum in the tropical Atlantic and a minimum in the tropical Pacific. The wave-1 pattern is driven by injection of lightning NO into the upper troposphere over the tropical continents, followed by photochemical production of NO_2, HNO_3, and O_3 during transport to the tropical Atlantic as part of the Walker Circulation. The lightning signal over the tropical Atlantic and Africa was $2–6 \times 10^{14}$ molecules NO_2 cm^{-2}, 15 Dobson Units of O_3, and 125 pptv HNO_3, as determined by the difference between the standard simulation with 6 Tg N yr^{-1} from lightning and a simulation without lightning NO_x emissions. The lightning signal over the tropical Pacific was 25–75% weaker.

[42] Sensitivity simulations were conducted with the GEOS-Chem model for lightning NO_x emissions of 0, 4, 6, and 8 Tg N yr^{-1}. The simulations were sampled at the same locations and times as the satellite observations. Comparison of these simulations with the satellite observations reveals that it is very likely that global lightning NO_x emissions are between 4 and 8 Tg N yr^{-1}. Emissions of 6 Tg N yr^{-1} provide the most consistent representation of the NO_2, HNO_3, and O_3 measurements. This conclusion is robust to scaling the spatial distribution of the simulated lightning NO_x production to flash count observations from the OTD and LIS instruments.

[43] Tropospheric O_3 columns provide a particularly strong constraint on the magnitude of lightning NO_x emissions due to their insensitivity to the relative vertical profile of lightning NO_x production, and due to the large lightning signal of 10–15 DU that is 2–3 times greater than the measurement uncertainty. Tropospheric NO_2 columns and upper tropospheric HNO_3 concentrations provide additional information on the vertical profile of lightning NO_x production. Increasing the altitude of lightning NO_x production reduces the tropospheric NO_2 column by increasing the NO/NO_2 ratio, while increasing the upper tropospheric HNO_3 concentration by reducing convective scavenging. A sensitivity simulation with enhanced intracloud lightning yields NO_2 columns that are half of those in the standard simulation and HNO_3 concentrations that are 50–100% larger than those in the standard simulation.

[44] This analysis could be improved in a number of ways. The lightning signal is comparable to the measurement uncertainty for tropospheric NO_2; a more accurate retrieval of this species would be particularly valuable. The ACE-FTS HNO_3 measurements remain sparse; additional measurements from the Tropospheric Emission Spectrometer (TES), the Microwave Limb Sounder (MLS), or the Interferometric Monitor for Greenhouse gases (IMG) instruments would be useful. Model development to better represent processes such as lightning, convection, pulsing of soil NO_x emissions, and uptake of HNO_3 on ice would improve the robustness of the constraint. Development of an adjoint model would provide a more formal approach to extend this analysis.

[45] **Acknowledgments.** We thank Folkert Boersma, Rynda Hudman, Ken Pickering, and three anonymous reviewers for helpful comments that

improved the manuscript. We are grateful to the Netherlands SCIAMACHY Data Center (NL-SCIA-DC) for providing data and processing services. This work was supported by NASA's Radiation Science Program. The ACE mission is supported by the Canadian Space Agency and the Natural Sciences and Engineering Research Council of Canada.

References

Abbatt, J. P. D. (1997), Interaction of HNO_3 with water-ice surface at temperatures of the free troposphere, *Geophys. Res. Lett.*, *24*, 1479–1482.

Alexander, B., J. Savarino, C. C. W. Lee, R. J. Park, D. J. Jacob, M. H. Thiemens, Q. B. Li, and R. M. Yantosca (2005), Sulfate formation in sea-salt aerosols: Constraints from oxygen isotopes, *J. Geophys. Res.*, *110*, D10307, doi:10.1029/2004JD005659.

Allen, D., and K. Pickering (2002), Evaluation of lightning flash rate parameterization for use in a global chemical transport model, *J. Geophys. Res.*, *107*(D23), 4711, doi:10.1029/2002JD002066.

Beirle, S., U. Platt, M. Wenig, and T. Wagner (2004), NO_x production by lightning estimated with GOME, *Adv. Space Res.*, *34*(4), 793–797.

Beirle, S., et al. (2006), Estimating the NOx produced by lightning from GOME and NLDN data: A case study in the Gulf of Mexico, *Am. Chem. Phys.*, *6*, 1075–1089.

Benkovitz, C. M., M. T. Scholtz, J. Pacyna, L. Tarrason, J. Dignon, E. C. Voldner, P. A. Spiro, J. A. Logan, and T. E. Graedel (1996), Global gridded inventories for anthropogenic emissions of sulfur and nitrogen, *J. Geophys. Res.*, *101*, 29,239–29,253.

Bernath, P. F., et al. (2005), Atmospheric Chemistry Experiment (ACE): Mission overview, *Geophys. Res. Lett.*, *32*, L15S01, doi:10.1029/2005GL022386.

Bey, I., et al. (2001), Global modeling of tropospheric chemistry with assimilated meteorology: Model description and evaluation, *J. Geophys. Res.*, *106*, 23,073–23,096.

Boccippio, D. J., K. L. Cummins, H. J. Christian, and S. J. Goodman (2001), Combined satellite- and surface-based estimation of the intra-cloud-cloud-to-ground lightning ratio over the continental United States, *Mon. Weather Rev.*, *129*, 108–122.

Boersma, K. F., H. J. Eskes, E. W. Meijer, and H. Kelder (2005), Estimates of lightning NOx production from GOME satellite observations, *Am. Chem. Phys.*, *5*, 2311–2331.

Bond, D. W., S. Steiger, R. Zhang, X. Tie, and R. E. Orville (2002), The importance of NOx production by lightning in the tropics, *Atmos. Environ.*, *36*, 1509–1519.

Boone, C. D., R. Nassar, K. Walker, Y. Rochon, S. D. McLeod, C. P. Rinsland, and P. F. Bernath, (2005), Retrievals for the atmospheric chemistry experiment Fourier-transform spectrometer, *Appl. Opt.*, *44*(33), 7218–7231.

Bovensmann, H., J. P. Burrows, M. Buchwitz, J. Frerick, V. V. Rozanov, K. V. Chance, and A. P. H. Goede (1999), SCIAMACHY: Mission objectives and measurement modes, *J. Atmos. Sci.*, *56*(2), 127–150.

Bradshaw, J., et al. (1999), Photofragmentation two-photon laser-induced fluorescence detection of NO_2 and NO: Comparison of measurements with model results based on airborne observations during PEM-Tropics A, *Geophys. Res. Lett.*, *26*, 471–474.

Bucsela, E. J., E. A. Celarier, M. O. Wenig, J. F. Gleason, J. P. Veefkind, K. F. Boersma, and E. J. Brinksma (2006), Algorithm for NO_2 vertical column retrieval from the ozone monitoring instrument, *IEEE Trans. Geosci. Remote Sens.*, *44*, 1245–1258.

Chandra, S., J. R. Ziemke, P. K. Bhartia, and R. V. Martin (2002), Tropical tropospheric ozone: Implications for dynamics and biomass burning, *J. Geophys. Res.*, *107*(D14), 4188, doi:10.1029/2001JD000447.

Chandra, S., J. R. Ziemke, and R. V. Martin (2003), Tropospheric ozone at tropical and middle latitudes derived from TOMS/MLS residual: Comparison with a global model, *J. Geophys. Res.*, *108*(D9), 4291, doi:10.1029/2002JD002912.

Christian, H. J., et al. (2003), Global frequency and distribution of lightning as observed from space by the Optical Transient Detector, *J. Geophys. Res.*, *108*(D1), 4005, doi:10.1029/2002JD002347.

Cooper, O. R., et al. (2006), Large upper tropospheric ozone enhancements above mid-latitude North America during summer: In situ evidence from the IONS and MOZAIC ozone monitoring network, *J. Geophys. Res.*, *111*, D24S05, doi:10.1029/2006JD007306.

DeCaria, A. J., K. E. Pickering, G. L. Stenchikov, J. R. Scala, J. L. Stith, J. E. Dye, B. A. Ridley, and P. Laroche (2000), A cloud-scale model study of lighting-generated NO_x in an individual thunderstorm during STERAO-A, *J. Geophys. Res.*, *105*, 11,601–11,616.

DeCaria, A. J., K. E. Pickering, G. L. Stenchikov, and L. E. Ott, (2005), Lightning-generated NOx and its impact on tropospheric ozone production: A three-dimensional modeling study of a Stratosphere-Troposphere Experiment: Radiation, Aerosols and Ozone (STERAO-A) thunderstorm, *J. Geophys. Res.*, *110*, D14303, doi:10.1029/2004JD005556.

Duncan, B. N., R. V. Martin, A. C. Staudt, R. M. Yevich, and J. A. Logan (2003), Interannual and seasonal variability of biomass burning emissions constrained by remote-sensed observations, *J. Geophys. Res.*, *108*(D2), 4100, doi:10.1029/2002JD002378.

Edwards, D. P., et al. (2003), Tropospheric ozone over the tropical Atlantic: A satellite perspective, *J. Geophys. Res.*, *108*(D8), 4237, doi:10.1029/2002JD002927.

Evans, M. J., and D. J. Jacob (2005), Impact of new laboratory studies of N_2O_5 hydrolysis on global model budgets of tropospheric nitrogen oxides, ozone, and OH, *Geophys. Res. Lett.*, *32*, L09813, doi:10.1029/2005GL022469.

Fairlie, T. D., D. J. Jacob, and R. J. Park (2006), The impact of transpacific transport of mineral dust in the United States, *Atmos. Environ.*, *41*(6), 1251–1266.

Fehr, T., H. Holler, and H. Huntrieser (2004), Model study on production and transport of lightning-produced NOx in a EULINOX supercell storm, *J. Geophys. Res.*, *109*, D09102, doi:10.1029/2003JD003935.

Fiore, A. M., D. J. Jacob, I. Bey, R. M. Yantosca, B. D. Field, and J. G. Wilkinson (2002), Background ozone over the United States in summer: Origin and contribution to pollution episodes, *J. Geophys. Res.*, *107*(D15), 4275, doi:10.1029/2001JD000982.

Fishman, J., and V. G. Brackett (1997), The climatological distribution of tropospheric ozone derived from satellite measurements using version 7 Total Ozone Mapping Spectrometer and Stratospheric Aerosol and Gas Experiment data sets, *J. Geophys. Res.*, *102*, 19,275–19,278.

Fishman, J., C. E. Watson, J. C. Larsen, and J. A. Logan (1990), Distribution of tropospheric ozone determined from satellite data, *J. Geophys. Res.*, *95*, 3599–3617.

Folkins, I., M. Loewenstein, J. Podolske, S. J. Oltmans, and M. Profitt (1999), A barrier to vertical mixing at 14 km in the tropics: Evidence from ozonesondes and aircraft observations, *J. Geophys. Res.*, *104*, 22,095–22,102.

Folkins, I., P. Bernath, C. Boone, L. J. Donner, A. Eldering, G. Lesins, R. V. Martin, B.-M. Sinnhuber, and K. Walker (2006), Testing convective parameterizations with tropical measurements of HNO_3, CO, H_2O, and O_3: Implications for the water vapor budget, *J. Geophys. Res.*, *111*, D23304, doi:10.1029/2006JD007325.

Froidevaux, L., et al. (2006), Early validation analyses of atmospheric profiles from EOS MLS on the Aura satellite, *IEEE Trans. Geosci. Remote Sens.*, *44*, 1106–1121, doi:10.1109/TGRS.2006.864366.

Gallardo, L., and V. Cooray (1996), Could cloud-to-cloud discharges be as effective as cloud-to-ground discharges in producing NOx?, *Tellus, Ser. B*, *48*, 641–651.

Gao, R. S., et al. (2004), Evidence that nitric acid increases relative humidity in low-temperature cirrus clouds, *Science*, *303*, 516–520.

Highwood, E. J., and B. J. Hoskins (1998), The tropical tropopause, *Q. J. R. Meteorol. Soc.*, *124*, 1579–1604.

Hudman, R., et al. (2007), Surface and lightning sources of nitrogen oxides over the United States: magnitudes, chemical evolution, and outflow, *J. Geophys. Res.*, doi:10.1029/2006JD007912, in press.

Hudson, R. D., and A. M. Thompson (1998), Tropical tropospheric ozone from total ozone mapping spectrometer by a modified residual method, *J. Geophys. Res.*, *103*, 22,129–22,145.

Huntrieser, H., H. Schlager, C. Feigl, and H. Holler (1998), Transport and production of NOx in electrified thunderstorms–Survey of previous studies and new observations at midlatitudes, *J. Geophys. Res.*, *103*, 28,247–28,264.

Huntrieser, H., et al. (2002), Airborne measurements of NO_x, tracer species, and small particles during the European Lightning Nitrogen Oxides Experiment, *J. Geophys. Res.*, *107*(D11), 4113, doi:10.1029/2000JD000209.

Huntrieser, H., H. Schlager, H. Höller, U. Schumann, H. D. Betz, D. Boccippio, D. Brunner, C. Forster, and A. Stohl (2006), Lightning-produced NOx in tropical, subtropical and midlatitude thunderstorms: New insights from airborne and lightning observations, *Geophys. Res. Abstr.*, *8*, EGU06-A-03286.

Jacob, D. J. (2000), Heterogeneous chemistry and tropospheric ozone, *Atmos. Environ.*, *34*, 2131–2159.

Jacob, D. J., et al. (1996), Origin of ozone and NO_x in the tropical troposphere: A photochemical analysis of aircraft observations over the South Atlantic basin, *J. Geophys. Res.*, *101*, 24,235–24,250.

Jaeglé, L., D. J. Jacob, Y. Wang, A. J. Weinheimer, B. A. Ridley, T. L. Campos, G. W. Sachse, and D. Hagen (1998), Sources and chemistry of NOx in the upper troposphere over the central United States, *Geophys. Res. Lett.*, *25*, 1709–1712.

Jaeglé, L., et al. (2004), Satellite mapping of rain-induced nitric oxide emissions from soils, *J. Geophys. Res.*, *109*, D21310, doi:10.1029/2004JD004787.

Jaeglé, L., L. Steinberger, R. V. Martin, and K. Chance (2005), Global partitioning of NOx sources using satellite observations: Relative roles

of fossil fuel combustion, biomass burning and soil emissions, *Faraday Disc.*, *130*, 407–423, doi:10.1039/b502128.

Jenkins, G. S., K. Mohr, V. R. Morris, and O. Arino (1997), The role of convective processes over the Zaire-Congo Basin to the southern hemispheric ozone maximum, *J. Geophys. Res.*, *102*, 18,963–18,980.

Jing, P., D. M. Cunnold, E.-S. Yang, and H.-J. Wang (2005), Influence of isentropic transport on seasonal ozone variations in the lower stratosphere and subtropical upper troposphere, *J. Geophys. Res.*, *110*, D10110, doi:10.1029/2004JD005416.

Kasibhatla, P. S., H. Levy, W. J. Moxim, and W. L. Chameides (1991), The relative importance of stratospheric photochemical production on tropospheric NO_y levels: A model study, *J. Geophys. Res.*, *96*, 18,631–18,646.

Kim, J. H., S. Na, M. J. Newchurch, and R. V. Martin (2005), Tropical tropospheric ozone morphology and seasonality seen in satellite, model, and in-situ measurements, *J. Geophys. Res.*, *110*, D02303, doi:10.1029/2003JD004332.

Kley, D., P. J. Crutzen, H. G. J. Smit, H. Vömel, S. J. Oltmans, H. Grassl, and V. Ramanathan (1996), Observations of near-zero ozone concentrations over the convective Pacific: Effects on air chemistry, *Science*, *274*, 230–233.

Labrador, L. J., R. von Kuhlmann, and M. G. Lawrence (2005), The effects of lightning-produced NOx and its vertical distribution on atmospheric chemistry: Sensitivity simulations with MATCH-MPIC, *Am. Chem. Phys.*, *5*, 1815–1834.

Lamarque, J.-F., G. P. Brasseur, P. G. Hess, and J.-F. Müller (1996), Three-dimensional study of the relative contributions of the different nitrogen sources in the troposphere, *J. Geophys. Res.*, *101*, 22,955–22,968.

Lee, D. S., I. Köhler, E. Grobler, F. Rohrer, R. Sausen, L. Gallardo-Klenner, J. H. J. Olivier, F. J. Dentener, and A. F. Bouwman (1997), Estimations of global NO_x emissions and their uncertainties, *Atmos. Environ.*, *31*, 1735–1749.

Lelieveld, J., and P. J. Crutzen (1994), Role of deep cloud convection in the ozone budget of the troposphere, *Science*, *264*, 1759–1761.

Levelt, P. F., G. H. J. van den Oord, M. R. Dobber, A. Mslkki, H. Visser, J. Vries, P. Stammes, J. O. V. Lundell, and H. Saari (2006), The Ozone Monitoring Instrument, *IEEE Trans. Geosci. Remote Sens.*, *44*, 1093–1101, doi:10.1109/TGRS.2006.872333.

Levy, H., W. J. Moxim, and P. S. Kasibhatla (1996), A global three-dimensional time-dependent lightning source of tropospheric NO_x, *J. Geophys. Res.*, *101*, 22,911–22,922.

Levy, H., W. J. Moxim, A. A. Klonecki, and P. S. Kasibhatla (1999), Simulated tropospheric NO_x: Its evaluation, global distribution and individual source contributions, *J. Geophys. Res.*, *104*, 26,279–26,306.

Li, Q., et al. (2001), A tropospheric ozone maximum over the Middle East, *Geophys. Res. Lett.*, *28*, 3235–3238.

Li, Q., D. J. Jacob, T. D. Fairlie, H. Liu, R. M. Yantosca, and R. V. Martin (2002), Stratospheric versus pollution influences on ozone at Bermuda: Reconciling past analyses, *J. Geophys. Res.*, *107*(D22), 4611, doi:10.1029/2002JD002138.

Liu, X., et al. (2006), First directly-retrieved global distribution of tropospheric column ozone: Comparison with the GEOS-CHEM model, *J. Geophys. Res.*, *111*, D02308, doi:10.1029/2005JD006564.

Martin, R. V., et al. (2002a), An improved retrieval of tropospheric nitrogen dioxide from GOME, *J. Geophys. Res.*, *107*(D20), 4437, doi:10.1029/2001JD001027.

Martin, R. V., et al. (2002b), Interpretation of TOMS observations of tropical tropospheric ozone with a global model and in-situ observations, *J. Geophys. Res.*, *107*(D18), 4351, doi:10.1029/2001JD001480.

Martin, R. V., D. J. Jacob, K. Chance, T. P. Kurosu, P. I. Palmer, and M. J. Evans (2003a), Global inventory of nitrogen oxide emissions constrained by space-based observations of NO_2 columns, *J. Geophys. Res.*, *108*(D17), 4537, doi:10.1029/2003JD003453.

Martin, R. V., D. J. Jacob, R. M. Yantosca, M. Chin, and P. Ginoux (2003b), Global and regional decreases in tropospheric oxidants from photochemical effects of aerosols, *J. Geophys. Res.*, *108*(D3), 4097, doi:10.1029/2002JD002622.

Martin, R. V., et al. (2006), Evaluation of space-based constraints on nitrogen oxide emissions with regional aircraft measurements over and downwind of eastern North America, *J. Geophys. Res.*, *111*, D15308, doi:10.1029/2005JD006680.

Moxim, W. J., and H. Levy (2000), Model analysis of the tropical South Atlantic Ocean tropospheric ozone maximum: The interaction of transport and chemistry, *J. Geophys. Res.*, *105*, 17,393–17,415.

Murphy, D., D. Fahey, M. Proffitt, S. Liu, C. Eubank, S. Kawa, and K. Kelly (1993), Reactive odd nitrogen and its correlation with ozone in the lower stratosphere and upper troposphere, *J. Geophys. Res.*, *98*, 8751–8773.

Nesbitt, S. W., R. Zhang, and R. E. Orville (2000), Seasonal and global NO_x production by lightning estimated from the Optical Transient Detector (OTD), *Tellus, Ser. B*, *52*, 1206–1215.

Ott, L. E., K. E. Pickering, G. L. Stenchikov, H. Huntrieser, and U. Schumann (2007), The effects of lightning NO_x production during the July 21 EULINOX storm studied with a 3-D cloud-scale chemical transport model, *J. Geophys. Res.*, *111*, D0S307, doi:10.1029/2006JD007365.

Park, R. J., D. J. Jacob, M. Chin, and R. V. Martin (2003), Sources of carbonaceous aerosols over the United States and implications for natural visibility conditions, *J. Geophys. Res.*, *108*(D12), 4355, doi:10.1029/2002JD003190.

Park, R. J., D. J. Jacob, B. D. Field, R. M. Yantosca, and M. Chin (2004), Natural and transboundary pollution influences on sulfate-nitrate-ammonium aerosols in the United States: Implications for policy, *J. Geophys. Res.*, *109*, D15204, doi:10.1029/2003JD004473.

Penner, J. E., C. S. Athertson, J. Dignon, S. J. Ghan, J. J. Walton, and S. Hameed (1991), Tropospheric nitrogen: A three-dimensional study of sources, distributions, and deposition, *J. Geophys. Res.*, *96*, 959–990.

Pickering, K. E., Y. S. Wang, W. K. Tao, C. Price, and J. F. Muller (1998), Vertical distributions of lightning NO_x for use in regional and global chemical transport models, *J. Geophys. Res.*, *103*, 31,203–31,216.

Pickering, K. E., L. E. Ott, A. J. DeCaria, G. L. Stenchikov, D. J. Allen, and W.-K. Tao (2006), Using results from cloud-resolving models to improve lightning NO_x parameterizations for global chemical transport and climate models, *EOS Trans. AGU, Jt. Assem. Suppl.*, *87*(36), Abstract A52B-05.

Piotrowicz, S. R., H. F. Bezdek, G. R. Harvey, M. Springer-Young, and K. J. Hanson (1991), On the ozone minimum over the equatorial Pacific Ocean, *J. Geophys. Res.*, *96*, 18,679–18,687.

Price, C., and D. Rind (1992), A simple lightning parameterization for calculating global lightning distributions, *J. Geophys. Res.*, *97*, 9919–9933.

Price, C., and D. Rind (1994), Possible implications of global climate change on global lightning distributions and frequencies, *J. Geophys. Res.*, *99*, 10,823–10,831.

Price, C., J. Penner, and M. Prather (1997a), NO_x from lightning: 1. Global distribution based on lightning physics, *J. Geophys. Res.*, *102*, 5929–5941.

Price, C., J. Penner, and M. Prather (1997b), NO_x from lightning: 2. Constraints from the global atmospheric electric circuit, *J. Geophys. Res.*, *102*, 5943–5951.

Richter, A., and J. P. Burrows (2002), Tropospheric NO_2 from GOME measurements, *Adv. Space Res.*, *29*(11), 1673–1683.

Ridley, B. A., J. E. Dye, J. G. Walega, J. Zheng, F. E. Grahek, and W. Rison (1996), On the production of active nitrogen by thunderstorms over New Mexico, *J. Geophys. Res.*, *101*, 20,985–21,005.

Ridley, B., et al. (2004), Florida thunderstorms: A faucet of reactive nitrogen to the upper troposphere, *J. Geophys. Res.*, *109*, D17305, doi:10.1029/2004JD004769.

Ridley, B. A., K. E. Pickering, and J. E. Dye (2005), Comments on the parameterization of lightning-produced NO in global chemistry-transport models, *Atmos. Environ.*, *39*, 6184–6187.

Sauvage, B., V. Thouret, A. M. Thompson, J. C. Witte, J.-P. Cammas, P. Nedelec, and G. Athier (2006), Enhanced view of the "tropical Atlantic ozone paradox" and "zonal wave one" from the in situ MOZAIC and SHADOZ data, *J. Geophys. Res.*, *111*, D01301, doi:10.1029/2005JD006241.

Sauvage, B., R. V. Martin, A. van Donkelaar, X. Liu, K. Chance, L. Jaeglé, P. I. Palmer, S. Wu, and T.-M. Fu (2007a), Remote sensed and in situ constraints on processes affecting tropical tropospheric ozone, *Am. Chem. Phys.*, *7*, 815–838.

Sauvage, B., R. V. Martin, A. van Donkelaar, and J. R. Ziemke (2007b), Quantification of the factors controlling tropical tropospheric ozone and the South Atlantic maximum, *J. Geophys. Res.*, doi:10.1029/2006JD008008, in press.

Schoeberl, M. R., et al. (2004), Earth observing systems benefit atmospheric research, *EOS Trans. AGU*, *85*, 177–178.

Shiotani, M. (1992), Annual, quasi-biennial and El Niño-Southern Oscillation (ENSO) timescale variations in equatorial total ozone, *J. Geophys. Res.*, *97*, 7625–7633.

Skamarock, W. C., J. E. Dye, E. Defer, M. C. Barth, J. L. Stith, B. A. Ridley, and K. Baumann (2003), Observational- and modeling-based budget of lightning-produced NO_x in a continental thunderstorm, *J. Geophys. Res.*, *108*(D10), 4305, doi:10.1029/2002JD002163.

Thompson, A. M., K. E. Pickering, D. P. Menamara, M. R. Schoeberl, R. D. Hudson, J. H. Kim, E. V. Browell, V. W. J. H. Kirchoff, and D. Nganga (1996), Where did tropospheric ozone over southern Africa and the tropical Atlantic come from in October 1992?–Insights from TOMS, GTE TRACE A, and SAFARI 1992, *J. Geophys. Res.*, *101*, 24,251–24,278.

Thompson, A. M., B. G. Doddridge, J. C. Witte, R. D. Hudson, W. T. Luke, J. E. Johnson, B. J. Johnson, S. J. Oltmans, and R. Weller (2000), A tropical Atlantic paradox: Shipboard and satellite views of a tropospheric ozone maximum and wave-one in January-February 1999, *Geophys. Res. Lett.*, *27*, 3317–3320.

Thompson, A. M., et al. (2003), The 1998–2000 SHADOZ (Southern Hemisphere ADditional Ozonesondes) Tropical Ozone Climatology:

1. Comparison with TOMS and ground-based measurements, *J. Geophys. Res.*, *108*(D2), 8238, doi:10.1029/2001JD000967.

Toenges-Schuller, N., et al. (2006), Global distribution pattern of anthropogenic nitrogen oxide emissions: Correlation analysis of satellite measurements and model calculations, *J. Geophys. Res.*, *111*, D05312, doi:10.1029/2005JD006068.

Ullerstam, M., T. Thornberry, and J. P. D. Abbatt (2005), Uptake of gas-phase nitric acid to ice at low partial pressures: Evidence for unsaturated surface coverage, *Faraday Disc.*, *130*, 211–226.

Velders, G. J. M., C. Granier, R. W. Portmann, K. Pfeilsticker, M. Wenig, T. Wagner, U. Platt, A. Richter, and J. P. Burrows (2001), Global tropospheric NO_2 column distributions: Comparing 3-D model calculations with GOME measurements, *J. Geophys. Res.*, *106*, 12,643–12,660.

von Kuhlmann, R., and M. G. Lawrence (2006), The impact of ice uptake of nitric acid on atmospheric chemistry, *Atmos. Chem. Phys.*, *6*, 225–235.

Wang, H., A. W. Desilva, G. C. Goldenbaum, and R. R. Dickerson (1998), Nitric oxide production by simulated lightning–Dependence on current, energy, and pressure, *J. Geophys. Res.*, *103*, 19,149–19,159.

Wang, Y., D. J. Jacob, and J. A. Logan (1998), Global simulation of tropospheric O_3-NO_x-hydrocarbon chemistry: 1. Model formulation, *J. Geophys. Res.*, *103*, 10,713–10,726.

Waters, J. W., et al. (2006), The Earth Observing System Microwave Limb Sounder (EOS MLS) on the Aura satellite, *IEEE Trans. Geosci. Remote Sens.*, *44*, 1075–1092, doi:10.1109/TGRS.2006.873771.

Yienger, J. J., and H. Levy (1995), Empirical model of global soil-biogenic NO_x emissions, *J. Geophys. Res.*, *100*, 11,447–11,464.

Zhang, X., J. H. Helsdon, and R. D. Farley (2003), Numerical modeling of lightning-produced NO_x using an explicitly lightning scheme: Two-dimensional simulation as a "proof of concept", *J. Geophys. Res.*, *109*(D18), 4579, doi:10.1029/2002JD003224.

Ziemke, J. R., and S. Chandra (1999), Seasonal and interannual variabilities in tropical tropospheric ozone, *J. Geophys. Res.*, *104*, 21,425–21,442.

Ziemke, J. R., S. Chandra, and A. M. Thompson (1996), Zonal asymmetries in southern hemisphere column ozone: Implications of biomass burning, *J. Geophys. Res.*, *101*, 14,421–14,427.

Ziemke, J. R., S. Chandra, B. N. Duncan, L. Froidevaux, P. K. Bhartia, P. F. Levelt, and J. W. Waters (2006), Tropospheric ozone determined from Aura OMI and MLS: Evaluation of measurements and comparison with the Global Modeling Initiative's Chemical Transport Model, *J. Geophys. Res.*, *111*, D19303, doi:10.1029/2006JD007089.

Zondlo, M. A., S. B. Barone, and M. A. Tolbert (1997), Uptake of HNO_3 on ice under upper tropospheric conditions, *Geophys. Res. Lett.*, *24*, 1391–1394.

P. Bernath and C. Boone, Department of Chemistry, University of Waterloo, Waterloo, Ontario, N2L 3G1, Canada.

I. Folkins, R. V. Martin, and B. Sauvage, Department of Physics and Atmospheric Sciences, Dalhousie University, Halifax, Nova Scotia, B3H 3J5, Canada. (randall.martin@dal.ca)

C. E. Sioris, Environment Canada, 4905 Dufferin Street, Toronto, Ontario, M3H 5T4, Canada.

J. Ziemke, NASA Goddard Space Flight Center, Code 613.3, Greenbelt, MD 20771, USA.